AIAA JOURNAL
Vol. 34, No. 7, July 1996

Trailing-Edge Jet Control of Leading-Edge Vortices of a Delta Wing

Chiang Shih* and Zhong Ding†
Florida A&M University and Florida State University, Tallahassee, Florida 32316-2175

The effect of using a trailing-edge jet to control the leading-edge vortices of a delta wing is investigated experimentally in a water towing tank facility. The Reynolds number, based on the freestream velocity and the root chord, is 9.8×10^3. Both static and dynamic (pitching-up) conditions are tested. For the dynamic cases, the wing is pitched from 10- to 45-deg angle of attack with pitch rates varied from 0.043 to 0.26. From the dye flow visualization, it is shown that a downward vectored trailing-edge jet can significantly delay the vortex breakdown on a delta wing. Strong asymmetric breakdown of the leading-edge vortices can be induced by arranging the vectored jet in an asymmetric configuration. Transient pitching motion delays the onset of the vortex breakdown. The initial delay is independent of the pitch rate. Also, the use of jet control is found to be effective for the dynamic cases. During the initial pitching-up period, the use of jet control has a dominant influence on the propagation of the vortex breakdown. In general, with jet control, the propagation of the vortex breakdown slows down. From instantaneous particle image velocimetry measurements, a quasiperiodic variation of the leading-edge vorticity field is detected before the vortex breakdown. This variation appears to relate to the strong interaction between the separating shear layer, the secondary vortex, and the primary vortex. Along the vortex axis, the velocity distribution changes from a jet-type profile to a wake-type profile, signifying the onset of vortex breakdown.

Nomenclature

A_j	= total areas of both jet nozzles
A_w	= surface area of the delta wing
C	= root chord
C_j	= jet momentum coefficient, $\rho U_j^2 A_j / \rho U_\infty^2 A_w$
Re	= Reynolds number
t^+	= nondimensionalized time, tU_∞ / C
U_j	= control jet velocity
U_p	= propagation velocity of the vortex breakdown location
U_∞	= freestream velocity
v, w	= velocity components in (y, z) coordinate system
X_b	= vortex breakdown location
x, y, z	= coordinate system
x', y', z'	= coordinate system with reference to the vortex core plane
α	= angle of attack
α_j	= angle of the control jet
α^+	= nondimensionalized pitch rate, $\dot{\alpha} C / U_\infty$
$\dot{\alpha}$	= pitch rate
Γ	= circulation

Introduction

CURRENT interest in the development of highly maneuverable fighter aircraft has prompted extensive study of the flow past a delta wing.[1-3] The most distinguishing feature of the delta wing flowfield is the existence of a pair of well-organized and highly energetic counter-rotating leading-edge vortical structures. These vortices form at a moderate angle of attack (AOA) as a result of flow separation along the delta wing sharp leading edges. The leading-edge vortex flow induces a large suction force on the delta wing surface and enhances the overall performance of the aircraft. These leading-edge vortices over the delta wing remain robust even at relatively high AOA when most of the conventional unswept wings encounter stall. Because of these performance aspects, the delta wing is the most widely used generic form for the study of flight aerodynamics. Unfortunately, at a high AOA, the vortices develop a large-scale instability that is characterized by rapid deceleration and eventual stagnation of the axial velocity along the vortex core, which leads to strong oscillation and total breakdown of the vortical structure. This phenomenon is commonly known as vortex breakdown, or vortex burst. After breakdown, the leading-edge vortices lose their effectiveness in generating lift. In addition, the ensuing flow unsteadiness associated with vortex breakdown generates buffet on the wing, resulting in a deterioration of the quality of aerodynamic control. For decades, considerable efforts had been made in trying to understand the physical mechanism of vortex breakdown.[4-6] Significant progress had been achieved and reviewed extensively by Hall[7] and more recently by Leibovich.[8] However, a universally accepted theory that can account for the mechanism of vortex breakdown has not yet been developed. To make the matter more complicated, the onset of the vortex breakdown is greatly affected by the pitching motion during a high AOA maneuver. It was discovered that rapid pitching motion always resulted in drastically different flow behavior compared with that of a quasisteady flow. Substantial delay of the vortex breakdown and the associated improvement of aerodynamic performance were consistently observed both experimentally[9,10] and numerically.[11,12] However, despite these recent efforts, these added unsteady effects are still poorly understood. Therefore, to achieve a controllable poststall maneuver, a fundamental understanding of the mechanism of the leading-edge vortex flowfield, under both static and dynamic conditions, is necessary.

The maneuverability of modern fighter aircraft is achieved primarily through the use of leading- or trailing-edge devices. During flight maneuvers, these devices are exposed to unsteady flow that limits their operational performance. In addition, the response of these mechanical devices is usually not fast enough at high-speed and high AOA conditions. One alternative for replacing these control devices is to integrate the aircraft propulsive and lift systems. It has been demonstrated that a thin jet sheet deflected from an airfoil's trailing edge could be used in place of a mechanical flap to achieve a high lift coefficient.[13] The jet flap, as the configuration is called, offers many advantages in both low- and high-speed flight regimes. The application of an aeropropulsion integration using exhaust nozzles can increase lift as a result of the induced aerodynamics created by the nozzle exhaust flow near the trailing edge. Moreover, the instantaneous maneuvering capability can also be improved by using a vectoring exhaust jet. These benefits are directly related to the interaction between the wing aerodynamics and the jet flowfield.

Received May 23, 1995; revision received Sept. 11, 1995; accepted for publication Nov. 14, 1995.

*Associate Professor, Department of Mechanical Engineering, College of Engineering. Member AIAA.
†Graduate Assistant, Department of Mechanical Engineering, College of Engineering.

A properly designed integration of the aeropropulsion system will greatly improve the performance of the aircraft. However, most of the previous studies[14,15] are oriented at studying high-lift devices for unswept wings and are confined to low AOA cases. As far as the effect of a trailing-edge vectored jet on the leading-edge vortex flow of the delta wing is concerned, very limited information[16–18] is available.

One of the reasons why the behavior of a leading-edge vortex flow is not well understood is because of the lack of comprehensive experimental information. Much of the information about the vortex breakdown process is acquired through the use of flow visualization techniques. Its effectiveness is limited when quantitative information on the flow is sought. On the other hand, the leading-edge vortex flow is extremely sensitive to the presence of small disturbances in the vortex core region. Therefore, the use of intrusive techniques such as conventional pressure probes and hot wires will inevitably disturb the flowfield and make the measurements highly unreliable. The situation has changed recently with the advance in optical diagnostic techniques such as laser Doppler anemometry (LDA) and particle image velocimetry (PIV). The use of these nonintrusive techniques allows a detailed investigation of the flow behavior inside the vortex core region, thus resulting in an improvement in the understanding of the leading-edge vortex flow. In particular, PIV can provide instantaneous whole-field velocity information in a selected flow plane with enough accuracy to resolve the vorticity field.[19,20] This is a significant aid in understanding the behavior of a leading-edge vortex.

The flowfield over a delta wing, under the influence of a vectored jet issuing from its trailing edge at both static and dynamic (pitching-up) conditions, is studied. Emphasis is placed on understanding the aerodynamic behavior of the basic flow structure (such as the breakdown of leading-edge vortices) of a pitching-up delta wing with the presence of thrust vectoring jets. PIV technique is used to complement the qualitative dye flow visualization studies.

Experimental Setup

The experiments are performed in a water towing tank facility with dimensions of 3.6 m in length and 0.55×0.42 m^2 in cross section. A computer-interfaced Anorail linear motor system is used to drive the towing carriage. This system allows for fine control of the towing velocity. The Reynolds number based upon the wing's root chord C and the freestream velocity can be varied from 5×10^3 to 2.5×10^4. The ramp-type pitching motion is provided by a yoke mechanism that is connected to a programmable stepping motor via gear-belt arrangement. All motions are coordinated using a desktop IBM PS/2 model 70 computer. Three moving platforms, one for model mounting, one for the rotating mirror system used to create the pulsed laser illumination, and the other for image recording, are synchronized using a gear-belt system (Fig. 1). A 200-W aquarium pump that is connected to a 0.11-m^3 reservoir tank is used for the trailing-edge jet flow control. Two rectangular jet nozzles, each with its own supply line, are located at the trailing edge of the wing for control purpose.

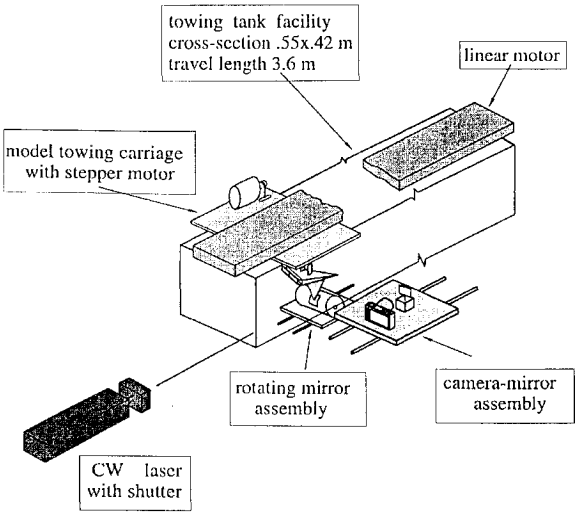

Fig. 1 Water towing tank facility and PIV photographic arrangement.

The delta wing model has a leading-edge sweep angle of 60 deg and a root chord of 13 cm. The Reynolds number, based on the freestream velocity of 7.48 cm/s, is 9.8×10^3 in all cases. The leading edges are beveled 45-deg leeward from the top surface. The model has a relatively large thickness of 2.54 cm (19.5% C) to accommodate the reservoir chambers of the trailing-edge jet. The model is mounted on its bottom surface using two stings. The Plexiglas® stings have the exterior shape of a NACA 0015 airfoil contour to minimize the interference generated by the sting supports. Inside each of the supports, a brass tube is used to direct the flow from the pump into the settling chamber for jet control. Two flow control systems are located symmetrically about the wing's centerline. The two control jets can be operated independently through a separate system of valves and passage conduits. To ensure a uniform jet output, the flow is expanded into the settling chamber filled with foam. No noticeable nonuniformity is observed based on visual inspection of the jet flow.

The direction of the jet flow is controlled by using two vectored nozzles mounted at the exit of the settling chamber. Each of the nozzles has a span of 4.89 cm and a height of 0.51 cm, which gives a 9.6 to 1 aspect ratio. Although the axis switching of the jet and the emergence of three-dimensionality is expected downstream, the near-jet flowfield is expected to be fairly two dimensional. By using different nozzle configurations, the deflection angle of the vectored jet system can be varied from 30-deg upward to 45-deg downward with respect to the upper surface of the wing. Currently, the jet velocity can be varied from 0 to 7.3 times U_∞. The strength of the jet is represented by the jet momentum coefficient C_j.

The term C_j can be varied from 0 to a maximum value of 1.11 in the present study. Except for the study of effects of jet velocity on vortex breakdown, all control cases were performed at the maximum jet velocity. The flow rate is determined by measuring the variation of the water level inside the reservoir tank over a period of time. The variation of the supply flow rate was less than 1% during each test.

PIV and Dye Flow Visualization Setup

For a qualitative understanding of the flow behavior, a dye flow visualization experiment is used. The development of the leading-edge vortex core is tagged by dye injected via small tubes near the apex of the delta wing. Initially, the dye is trapped inside the core when the leading-edge vortex is stable. The emergence of instabilities and the eventual breakdown of the vortex can be identified by the quick dispersion of the dye. A 35-mm Nikon camera, which is mounted on a platform moving with the wing, is used to record the flow visualization results for static cases. For the dynamic pitching cases, a video camera is used to achieve higher temporal resolution (30 frames/s). For the PIV measurements, the pulsed laser sheet is created by means of a 24-faceted rotating mirror system. This mirror sweeps an 18-W argon laser beam into discrete laser sheets that are projected along a selected plane on the wing, providing multiple particle image illumination required for PIV image recording.

The PIV technique is capable of providing two-dimensional, instantaneous velocity and vorticity fields with accuracy. Please refer to Lourenco et al.[21] for a detailed description. To resolve the directional ambiguity of the velocity vector, which may exist if flow reversal is present, a velocity bias technique is used. A uniform reference motion is added to the flow, thus superposing an image shift on the recorded film. A properly chosen shift can ensure that all image displacements occur in the same direction, thereby eliminating any ambiguity. The true flowfield can be recovered later by removing this artificial shift from the raw velocity data. In this work, a rotating mirror system is used to produce the image shift. A digital image processing technique is used to convert the acquired PIV photographic records into local velocity data. An optical scanner (Nikon Coolscan) is used to scan and digitize the PIV photographic film with a very high resolution of up to 106.4 pixels per millimeter. The digitized image can then be processed using a standard fast Fourier transform algorithm. In the present study, the PIV velocity field is computed locally using

a small interrogation window that has an equivalent physical dimension of 1.7×0.85 mm or $1.3 \times 0.7\%$ root chord length, respectively. The shorter side of the window is aligned in the direction normal to the freestream where the flowfield has a larger gradient. This PIV system has been implemented successfully in our laboratory to investigate highly unsteady and very complex flowfields such as the dynamic stall phenomenon of a pitching-up airfoil.[22]

Silver-coated hollow glass beads (Potter Industry), with an average diameter of 10 μm and a specific gravity of 1.3, are used as the flow tracers. A phase-triggered 35-mm SLR camera (Nikon F-3) is used to record the image at a controllable rate, ranging from 1 frame/s to a maximum rate of 6 frames/s. Synchronization between components is accomplished using a Counter/Timer processor interfaced to a Macintosh II computer. This system also provides the phase reference between the motion of the wing and the PIV photographic timing sequence.

Results and Discussion

Dye flow visualization experiments are carried out to study the dependence of vortex breakdown on various parameters, including the AOA, the pitch rate, and the effect of using trailing-edge jet control. The Reynolds number is set at 9.8×10^3. For the static cases, the AOA is varied from 10 to 35 deg in an increment of 5 deg. For the dynamic cases, the wing is pitched from 10- to 45-deg AOA using ramp-type pitching motion. The nondimensionalized pitch rate α^+ varies from 0.043 to 0.26. The trailing-edge vectored jet angle can be varied from 30-deg upward to 45-deg downward with respect to the delta wing surface, and the jet velocity can be varied from 0 to $7.3U_\infty$. Maximum jet flow is used in all control cases except for those cases where the effect of jet velocity are studied. Dye injected through tubes near the apex of the wing is used to tag the core of the leading-edge vortex. Initially, the dye is trapped inside the vortex core and the dye streak assumes a nearly straight line when the leading-edge vortex is stable. Because of the emergence of instability and eventual vortex breakdown, the dye streak becomes strongly oscillatory and quickly disperses away from the vortex core, where it can be easily identified from the flow visualization (Fig. 2). A light back and forth movement of the vortex breakdown location can be observed consistently at all high AOA (>10 deg). The amplitude of these oscillations seems to increase with increased AOA. The static AOA data presented are the averaged values of at least eight instantaneous vortex breakdown locations identified from the dye flow visualization. The vortex burst location is always measured downstream from the apex of the wing. The uncertainty for the static AOA cases is estimated to be within $\pm 2\%$ of the root chord.

Static Cases

The vortex bursts at approximately 50% chord location when the AOA is set at 15 deg (Fig. 2a). The bursting location gradually moves upstream to 12.5% chord from apex as the AOA is increased to 25 deg (Fig. 2b). A total breakdown of the vortices can be observed at an AOA of 35 deg. No distinguishable coherent vortical structure can be seen beyond this angle.

However, if the trailing-edge control jet is turned on, the bursting location can be changed significantly. The corresponding controlled case with C_j at 1.11 is presented in Figs. 2c and 2d. In this case, the trailing-edge jet is directed at 45-deg downward with respect to the wing. At an AOA of 15 deg, the leading-edge vortices stay unburst for the entire wing under control (Fig. 2c). As the AOA increases to 25 deg, the burst location moves to 50% chord (Fig. 2d).

From the vortex breakdown location vs static AOA plots (Fig. 3), it is obvious that there are significant disagreements between current data and previous works done by Wentz and Kohliman[23] and Miau et al.[24] To identify one possible source of this discrepancy, flow visualization tests have been repeated using a thinner (4.2% C) 60-deg delta wing model with otherwise identical configuration as the thick delta wing. The results, which are also presented in Fig. 3, compare favorable with other studies. This suggests that although other factors, such as different facilities, may also influence the results, it is most likely that the use of nonconventional thick (20% C) model is the primary cause for the discrepancy.

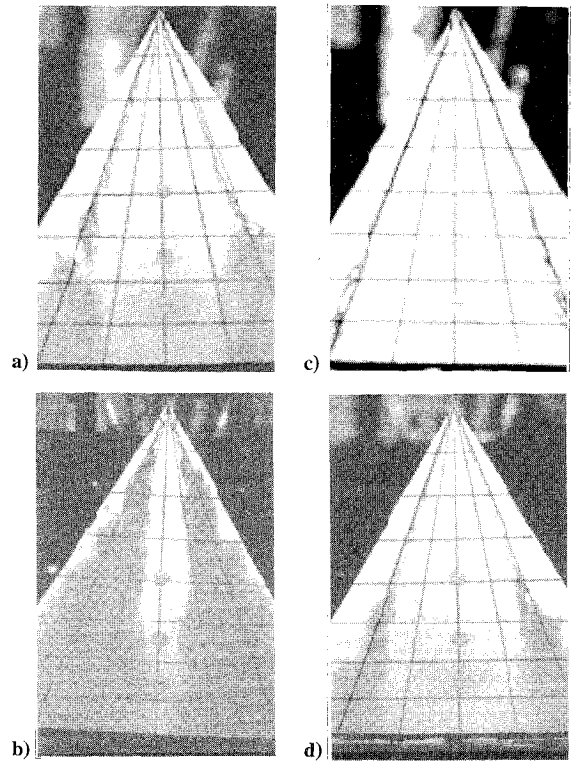

Fig. 2 Flow visualization result of a static delta wing. No control: a) AOA = 15 deg and b) AOA = 25 deg. With 45-deg downward jet control: c) AOA = 15 deg and d) AOA = 25 deg.

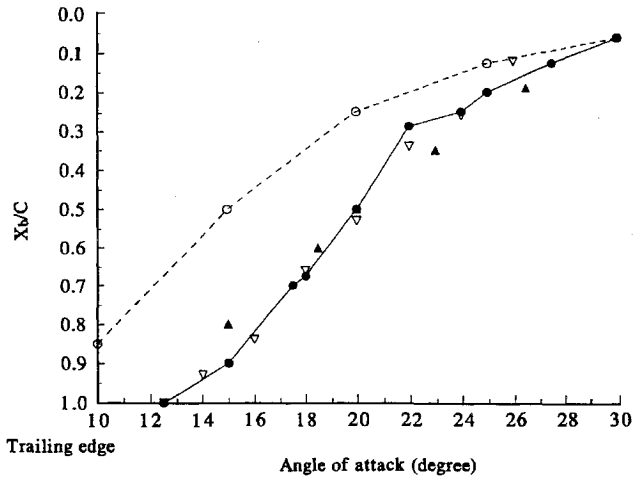

Fig. 3 Comparison of vortex breakdown location: ○, thick delta wing; •, thin delta wing; ▲, Wentz et al.[23]; and ▽, Miau et al.[24] (59 deg sweep).

Vectored Jet Angle

The effectiveness of using a vectoring jet to control vortex breakdown depends on several key factors that include the vectoring angle and the jet strength. The effect of vectoring angle on the vortex breakdown is studied by varying the vectoring angle of the trailing-edge jet from 15-deg upward to 45-deg downward. The jet velocity is set at the maximum level of $7.3U_\infty$ to produce the maximum effect. The results are presented in Fig. 4. The uncontrolled case is also included for comparison. For the uncontrolled case, the breakdown point moves very rapidly from 75 to 25% chord when the static angle is increased from 10 to 20 deg. If the angle is increased beyond 20 deg, the upstream propagation of the breakdown point becomes more gradual. The burst location changes from 25% chord from the apex to total breakdown as the angle is increased from 20 to 35 deg. This suggests that the wing-apex portion (first 25% chord) of the leading-edge vortex system is less susceptible to instabilities when the AOA is increased. All configurations of the vectored jet control, except the upward pointing jet case, show favorable effects

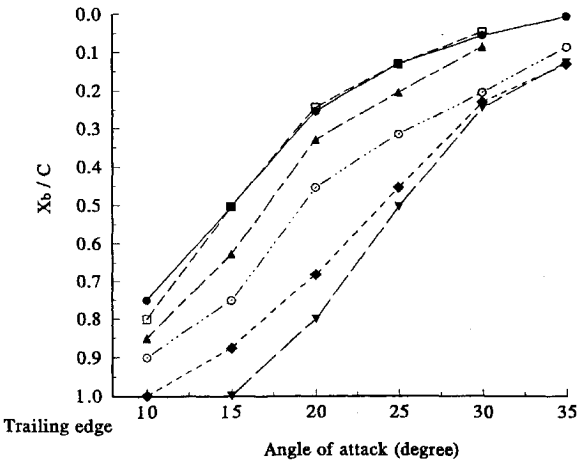

Fig. 4 Breakdown location vs AOA, static case, with symmetric trailing-edge jet control: ▲, 0-deg jet; •, 0-deg no jet; □, 15-deg upward jet, ○, 15-deg downward jet; ♦, 30-deg downward jet; and ▼, 45-deg downward jet.

on the vortex breakdown. The 15-deg upward control case shows no noticeable effect on the vortex breakdown as compared with the no control case. The 0-deg jet control case produces a consistent improvement of about 10% chord vortex breakdown delay at all AOA. As the jet angle increases, the delay of the vortex burst location is increased for all AOA tested. For example, at 20-deg AOA the burst location is moved from $X_b/C = 25\%$ for the uncontrolled case to 80% for the 45-deg downward control case. Within the range tested, the higher the downward jet angle, the more effective the control in delaying the vortex breakdown. However, this favorable effect due to higher downward jet angle seems to diminish quickly as the jet angle exceeds 30 deg. This suggests there is an upper limit for the vectored jet angle such that any increase beyond that angle may not produce further delays of vortex breakdown. Furthermore, the favorable effect generated as a result of the downward vectored jet angle diminishes quickly as the AOA increases. This is evident since the influence of the control jet is reduced as the vortex breakdown location moves further away from the trailing edge.

Asymmetric Control

As shown previously, downward vectoring control shows significant favorable effects, whereas the effect of upward control is minimum. This suggests that it is possible to control the two leading-edge vortices independently by arranging the control jet asymmetrically. In the present setup, the left-side jet is directed 30-deg downward relative to the wing, whereas the right-side jet is pointing 30-deg upward (Fig. 5). A dye flow visualization result at 25-deg AOA is also presented in Fig. 5. On the left side, the favorable pressure gradient produced by the downward vectored jet delays the vortex burst location to 35% chord from the apex. The right-side jet shows little favorable effect and the right-side vortex bursts at 12.5% chord. To show the effect of the asymmetric jet control for different AOA, the vortex breakdown location for all four different conditions (no control, symmetric control, downward and upward jet control) is plotted against the static AOA (Fig. 6). It is important to note that this asymmetric pattern due to asymmetric control remains stable throughout the experiment and is consistent for all AOA tested. This suggests that the asymmetric vortex breakdown produced by the trailing-edge jet is robust. As shown, the symmetric downward control configuration has the most favorable effect on the delay of vortex breakdown. For the asymmetric control case, the vortex breakdown position on the downward jet side is delayed for all AOA; however, the effect is less compared with the symmetric case except at either low (<10-deg) or high (>30-deg) AOA. This degraded performance is caused by the interference from the upward pointing jet located on the other side of the trailing edge. On the upward control side, no appreciable delay can be detected.

Vectored Jet Velocity

The effect of control also depends on the velocity of the trailing-edge jet. To study this effect, two symmetric jet control

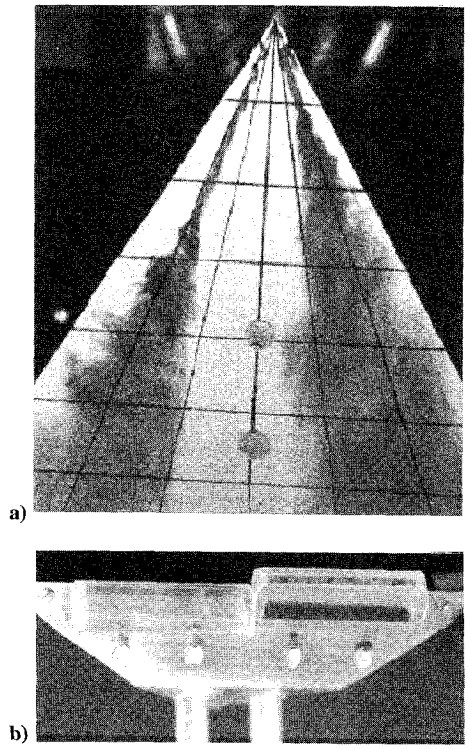

Fig. 5 Asymmetric trailing-edge jet control. Left-side jet, 30-deg downward and right-side jet, 30-deg upward. a) Flow visualization result of a static delta wing, AOA = 25 deg and b) trailing-edge nozzle configuration.

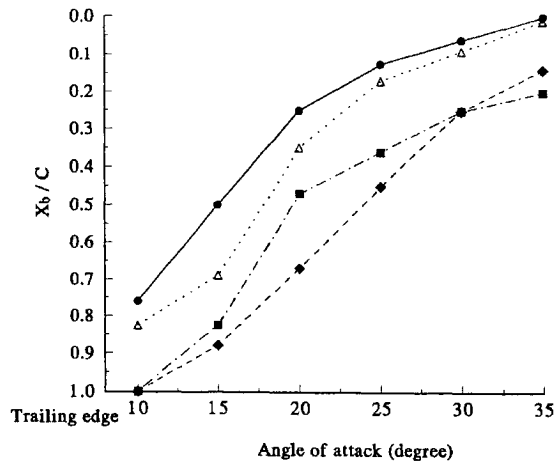

Fig. 6 Vortex breakdown location vs static AOA: •, no control; △, 30-deg upward asymmetric control; ■, 30-deg downward asymmetric control; and ♦, 30-deg downward asymmetric control.

configurations, a 0-deg angle case and a 45-deg downward angle case, are chosen. The delta wing's AOA is fixed at 20 deg. The jet velocity is varied from 0 to $7.3U_\infty$. Flow visualization results of vortex breakdown location for different jet velocities for both configurations are plotted in Fig. 7 (data set from Helin and Watry[17] is also included for comparison).

The effect of the 0-deg vectored jet control is limited. An increase in the jet velocity at this angle shows no noticeable delay of the breakdown location until $U_j/U_\infty > 5.0$. Even at the maximum jet velocity of $7.3U_\infty$, the delay is only about 9% chord. The 45-deg downward control case shows a more significant effect. First, no appreciable delay of the vortex breakdown is observed when the jet velocity is below a threshold limit of about $1.8U_\infty$. However, when the jet velocity is increased beyond this limit, the vortex breakdown location moves rapidly downstream. For example, at a velocity of $2.6U_\infty$, the vortex breakdown is delayed for more than 15% chord downstream. Within the range tested, this favorable effect continues,

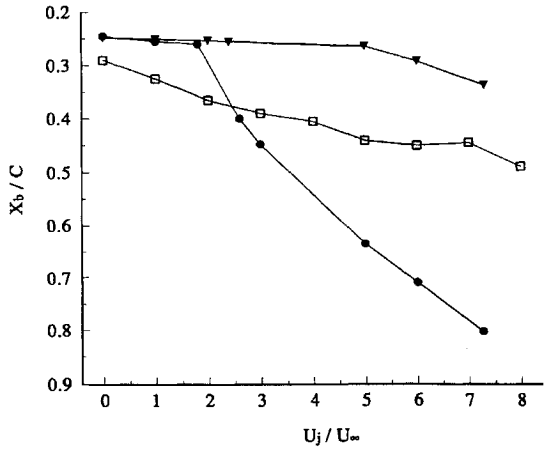

Fig. 7 Effect of trailing-edge jet velocity on vortex breakdown, AOA = 20 deg: H, 0-deg jet; †, 45-deg downward jet; and 2, data from Helin et al.[17]

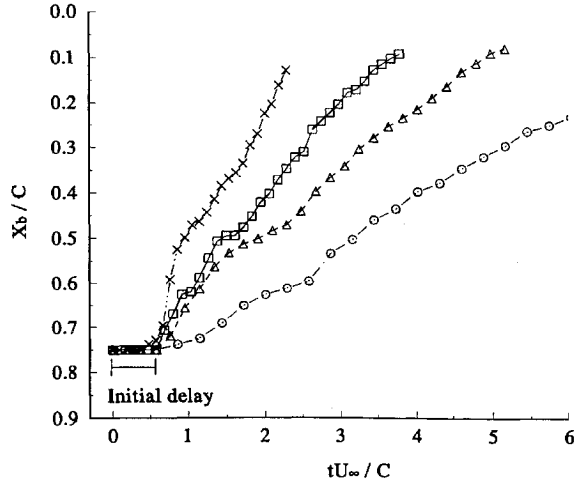

Fig. 8 Breakdown location vs time, no control, different pitch rates: –, pitch rate 0.043; M, pitch rate 0.086; 2, pitch rate 0.130; and £, pitch rate 0.260.

showing no sign of tapering off, as the jet velocity is increased. At the maximum jet velocity, the breakdown location is delayed 58% chord downstream.

The effect of trailing-edge jets has also been studied by Helin and Watry[17] who used a 0-deg jet nozzle configuration for control. Their results are also included in Fig. 7 for comparison. Their data show a consistently higher (more favorable) X_b/C value for the vortex breakdown location as compared with our 0-deg jet case. Although both groups use a 60-deg delta wing, our model is much thicker than theirs since an internal chamber is included inside the wing body for a smooth expansion of the trailing-edge jet. As mentioned before, it is speculated that the discrepancy in vortex breakdown location is mainly due to the difference in the thickness of the models.

The trailing-edge control jet creates a local streamwise favorable pressure gradient region near the trailing edge that tends to relieve the overall adverse pressure gradient imposed by the external flow. It is reasonable to argue that the favorable pressure gradient created by the trailing-edge jet depends on its strength or, in other words, the jet velocity. When the jet velocity is low, its favorable influence is only limited to a small local region, and its influence can not be felt upstream where the severe adverse pressure gradient dominates. Therefore, there is no delay of the vortex breakdown below a certain threshold limit.

Another interesting thing to note is the steadiness of the vortex axis angle that is defined as the angle between the centerline of the delta wing and the vortex axis (which can be clearly identified from the dye streak). The vortex axis always assumes a 19 § 1-deg angle and is essentially independent of the AOA of the delta wing, even under dynamic pitching conditions. Also, when the trailing-edge control jet is turned on, no significant change of the vortex axis angle can be observed except very close to the trailing edge where the dye streak is turned inside towards the centerline. This suggests that the flow separation at the leading edge of the delta wing is a robust process and is not easily subject to other influences. Although the trailing-edge jet has a significant effect on the leading-edge vortex flow, the vortex axis stays unchanged. The fact that the vortex core always stays on the same straight line is also important for measurement of the flow along the vortex core using PIV. It is therefore possible to project the illuminating laser sheet precisely along the entire vortex core.

Dynamic Pitching Cases

When the delta wing undergoes a transient pitching motion, a delay of the onset of vortex breakdown to a higher AOA as compared with static case is consistently observed. This delay is closely linked to the dynamic effect of the pitching motion. An experimental investigation of ramp-type pitch-up motion with a nondimensionalized pitch rate ranging from 0.043 to 0.26 is carried out to study the dynamic effect. The delta wing is pitched from an AOA of 10 to 45 deg. The wing accelerates at a constant rate to achieve its desired constant rotational speed in less than 6% of C/U_1 for all pitch rates tested. Similar to the static cases, the vortex breakdown location is measured from the apex of the delta wing. A video camera is used to record the flow visualization results. Its temporal resolution of 30 frames/s is sufficient to resolve the propagation of the instantaneous vortex breakdown location even for the highest pitch rate case, fiC D 0 26.

No Control

Figure 8 shows the progression of the vortex breakdown point with respect to the nondimensional time variation for pitching without jet control cases. When the delta wing first starts the ramp-type pitching motion, the vortex burst location appears to be unaffected by the movement for a period of time. Miau et al.[24] suggested that this delay is caused because the primary vortex can not respond instantaneously to the sudden change of the AOA and that its growth is lagging behind the initial ramp-up motion. As a result, this underdeveloped structure probably experiences a less severe adverse axial pressure gradient and can stay unburst longer as compared with a static case at the same AOA. If one accepts this argument, it is expected that the initial delay time should be correlated to the time required for the primary vortex to adjust itself to the newly changed flow condition. In other words, the delay should be closely linked to the time required for the newly generated vorticity from the leading edge to be entrained into the primary vortex. This delay should be relatively insensitive to the pitching rates (also shown by Ref. 24). It appears that, within the range tested in the present investigation, the initial delay is also independent of the pitch rates. However, the estimated initial delay of 0.58 is lower than the value of 1.0 obtained by other studies.[24] The difference is probably caused by the use of nonstandard (20% C thick) delta wing configuration in the present experiment. After the initial delay, the vortex breakdown location moves quickly upstream with a higher propagation speed, especially for the higher pitch rate cases. It is speculated that, because of the initial delay, the fully established leading-edge vortex experiences a more severe adverse pressure gradient since the wing has already pitched to a higher AOA. This adverse condition accelerates the upstream progression of the breakdown. As the breakdown moves further upstream, this progression appears to experience another slowdown, which has been attributed[24] to the interaction between the secondary vortex and the primary vortex. After the second delay, the vortex breakdown point resumes its upstream movement with a relatively constant speed for each pitch rate. The propagation speed can be estimated by least-square fitting the data points (excluding data points that correspond to the initial delay) from this figure, and the results are presented in Fig. 9 along with the controlled cases. It can be clearly seen that the higher the pitch rate, the faster the vortex breakdown propagates upstream. It approaches 29% of the freestream velocity for the highest pitch rate for the uncontrolled case. Other factors, such as the pitch rate induced camber effect,[25,26] may also contribute to the delay of vortex

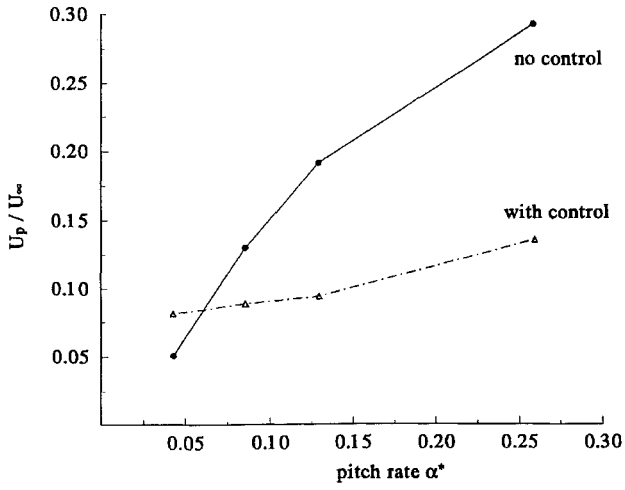

Fig. 9 Propagation velocity of the vortex breakdown location.

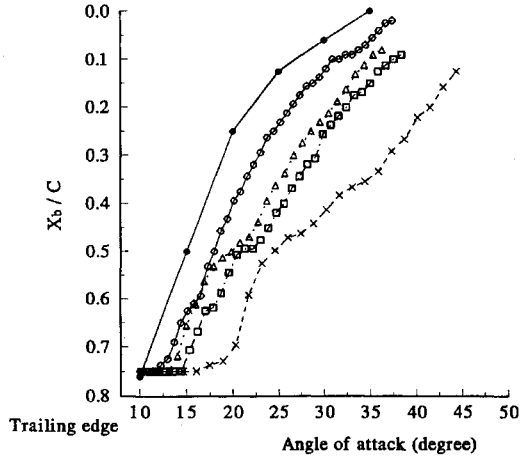

Fig. 10 Vortex breakdown location vs AOA, no control, different pitch rates: †, static AOA; –, pitch rate = 0.043; M, pitch rate = 0.086; 2, pitch rate = 0.13; and £, pitch rate = 0.26.

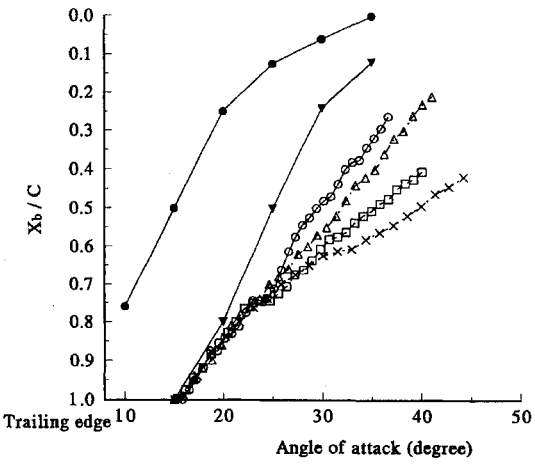

Fig. 11 Vortex breakdown location vs AOA, with 45-deg downward jet control, different pitch rates: †, static AOA; H, static AOA with control; –, pitch rate = 0.043; M, pitch rate = 0.086; 2, pitch rate = 0.130; and £, pitch rate = 0.260.

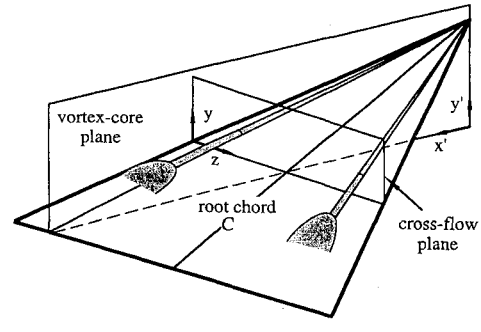

Fig. 12 Coordinate systems for PIV measurement.

breakdown. However, a comprehensive discussion of these effects is beyond the scope of the current works.

Note that the behavior of the dye streaks under unsteady conditions is more unpredictable compared with that of the static case. Therefore, it is more difficult to identify precisely the vortex breakdown location. This problem is especially serious during the initial pitching-up period. An uncertainty of § 3% chord for the estimation of the vortex breakdown location is expected.

The vortex breakdown progression vs AOA is presented in Fig. 10. For the lowest pitch rate of fi^c D 0 043, the trend of vortex breakdown position after the initial delay appears to match closely that of the static case. As the pitch rate is increased, the unsteady effect becomes increasingly dominant. For all AOA, there is always a higher percentage of the vortex stays unburst for a higher pitching rate case. For example, at the highest pitch rate, fi^c D 0 26, the vortex can stay unburst for about 35% chord length at 35-deg AOA. At this angle, the static case has already experienced total vortex breakdown.

With Jet Control

The use of trailing-edge jet control has been shown to be effective in delaying the leading-edge vortex breakdown process under static conditions. It is expected that the control system should produce a similar favorable effect under dynamic pitching-up motion. To examine this, a 45-deg downward vectoring nozzle configuration with a maximum jet velocity of $7.3U_1$ is used. The data are presented in Fig. 11. For comparison, data sets from static cases both with and without jet control are also included. The jet control is turned on before the initiation of the pitching-up motion to ensure a steady jet output. For all cases with jet control (both static and dynamic conditions), no vortex breakdown can be observed on the delta wing surface at AOA less than 15 deg. Beyond that angle, the breakdown point starts to move quickly upstream. However, it is interesting to note that, during the initial propagation period (X_b/C > 80%), all data for different pitch rates are essentially collapsed into one curve that also coincides closely with the data from the static with control case. This suggests that the breakdown process is dominated by the presence of jet control, for either static or dynamic conditions, as long as the vortex breakdown location remains close to the trailing edge. The dynamic effect becomes increasingly evident as all unsteady curves, including the lowest pitch rate case, start to deviate from the static one beyond 20-deg AOA. However, this dominant jet effect does not diminish until the wing pitches to AOA higher than 25 deg. Only after that, the unsteady effect for different pitch rates begins to show. For example, 45% of the vortex remains unburst at 45-deg AOA for the highest pitch rate (fi^c D 0 26), which is a dramatic improvement over the static uncontrolled case.

The use of jet control not only can delay the initiation of the vortex breakdown to a higher AOA, it also slows down the propagation of the breakdown process (see Fig. 9). Significant reductions of the propagation speed of the breakdown location are achieved for all but the lowest pitch rate (fi^c D 0 043) tested. For example, at the highest pitch rate, the propagation speed reduces from 29 to 14% freestream velocity when the control jet is used.

PIV Measurements

To provide a more quantitative understanding of the leading-edge vortex flow, PIV measurements are taken along selected planes. The first set includes several crossflow planes that are normal to the direction of the freestream, the y and z coordinates are directions normal to the freestream and parallel to the wing surface, respectively, with their origins fixed at the left side leading edge of the wing (Fig. 12). The second set of PIV measurement are taken along the vortex core plane that aligns with one of the vortex cores. The x^0 and y^0 are aligned in the horizontal and vertical direction, respectively, along the vortex core plane (Fig. 12). For all of the PIV cases presented

here, the delta wing is set at a fixed AOA of 12.5 deg. Several different crossflow sections, ranging from 50 to 92% root chord measured from the apex, are selected.

Crossflow Planes

From dye flow visualization, it is determined that at 12.5-deg AOA the vortex breaks down at about 63% root chord measured from the apex of the delta wing. At the cross section of 50% chord the vortex flow stays unburst with or without the control jet. Figures 13a and 13b show the ensemble-averaged (over 20 instantaneous ensembles) PIV velocity and associated iso-vorticity contour fields at this location with no control. Both the ensemble-averaged velocity and the vorticity fields show well-organized vortical structures. From Fig. 13a, it is clear that, different from a high sweep-angle slender delta wing, the velocity field is strongly asymmetric with respect to the vortex core as it has a very high outward velocity component (up to $1.5U_\infty$) close to the wing. By comparison, the inward velocity above the vortex core region is much slower and less than half of that value ($0.7U_\infty$). Consequently, underneath the primary vortex this strong outward flow stream induces a high level of reversed vorticity close to the wing surface. A strong secondary counter-rotating vortical structure is formed as a result of the separation of the outward flowing stream (Fig. 13b). The integrated circulation of the secondary vortex is approximately one-fifth of the primary vortex (-0.066 compared with 0.352). Considering the fact that the secondary vortex is more compact in size, it is clear that the secondary structure should have a comparable higher vorticity concentration compared with the primary vortex. The peak vorticity level measurement supports this observation (Fig. 13b). Furthermore, the close proximity of the secondary vortex to the separating shear layer at the edge of the wing also increases its influence on the development of the leading-edge vortex system. This aspect will be discussed in the following.

Figure 14 presents a sequence of three instantaneous flowfields with distinctive features, while the time is normalized by the freestream velocity and the root chord, $t^+ = tU_\infty/C$. In Fig. 14a, it can be seen that the instantaneous vortical structure is drastically different from the primary vortex, as characterized by the ensemble-averaged vorticity field (Fig. 13b). An elongated vortical structure, which consists of several highly concentrated vortical eddies, appears to be attached directly to the separated shear layer emanating from the edge of the delta wing (Fig. 14a). It is speculated that this connection enables the vortex to continuously receive a supply of vorticity from the shear layer. On the other hand, the close proximity of this structure to the surface induces an accumulation of a strong secondary counter-rotating vortex (dotted contour) underneath the primary structure. At the next instant (Fig. 14b), those individualized eddies inside the stretched structure appear to undergo a merging process and coalesce into one highly concentrated structure. Under the induction of the newly formed vortex, the secondary vortex is lifted up and penetrates through the link between the primary vortex and the separated shear layer. Because of the sudden termination of vorticity feeding from the shear layer and a continuous depletion of vorticity through downstream transportation, the primary vortical structure loses both its size and strength (Fig. 14c). As a result, the strength of the secondary vortex also subsides accordingly. This allows the reconnection of the primary vortex to the shear layer, and so the cycle repeats itself in a quasiperiodic fashion. Following from the preceding discussion, it appears that the secondary vortex actually plays an active role in the development of the leading-edge vortex system, instead of a secondary role as is commonly believed. It is important to note that the preceding discussion is only qualitative since the flow structure will not stay in the same crossflow plane; rather it will continue convecting downstream as time progresses. However, it is believed that the streamwise variation is not significant and all major features discussed earlier should be valid.

To further study the unsteady character of the leading-edge vortex system, a control volume is selected directly above the primary vortex core (as shown in Fig. 14b). The vorticity inside this control volume is integrated at each instant to obtain the circulation. This procedure is equivalent to measuring the variation of the local circulation by placing a vorticity probe in the flow with the size of the assigned control volume. A quasiperiodic variation is clearly shown in the circulation vs time plot (Fig. 15). For the purpose of reference, the three instantaneous vorticity fields presented in Fig. 14 are indicated as a–c at their corresponding time instants. The estimated Strouhal number, based on the freestream velocity and the root chord, is 2.1. This oscillation appears to be in the same Strouhal number range of the coherent fluctuations detected is

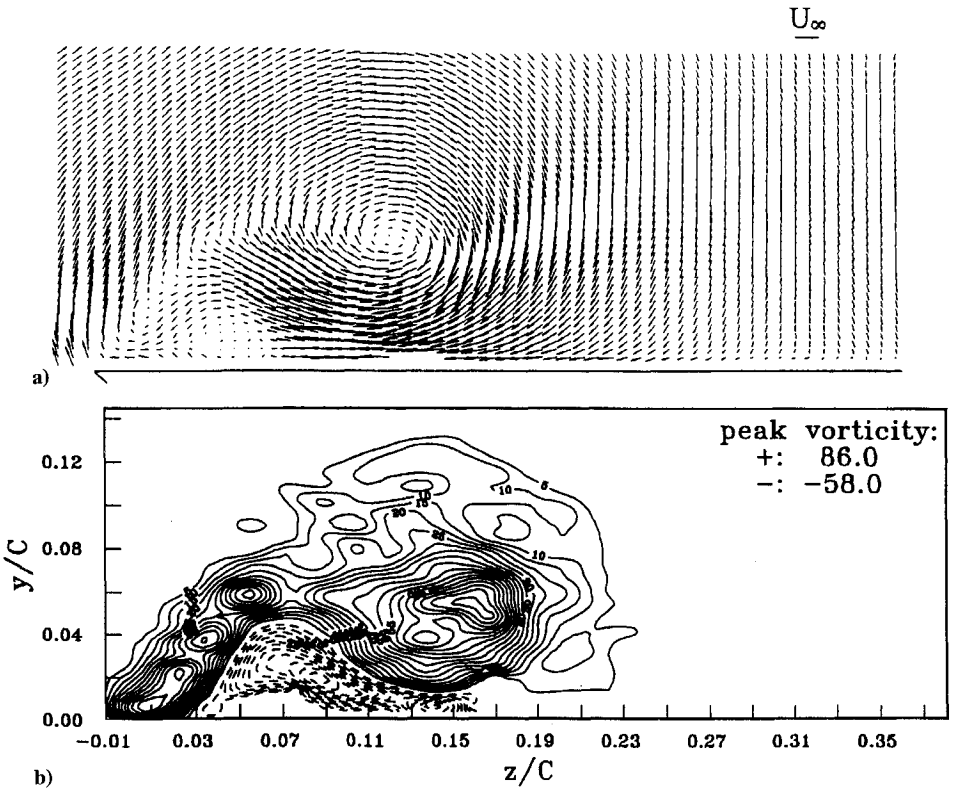

Fig. 13 Averaged a) velocity and b) vorticity fields at 50% chord from the apex, AOA = 12.5 deg.

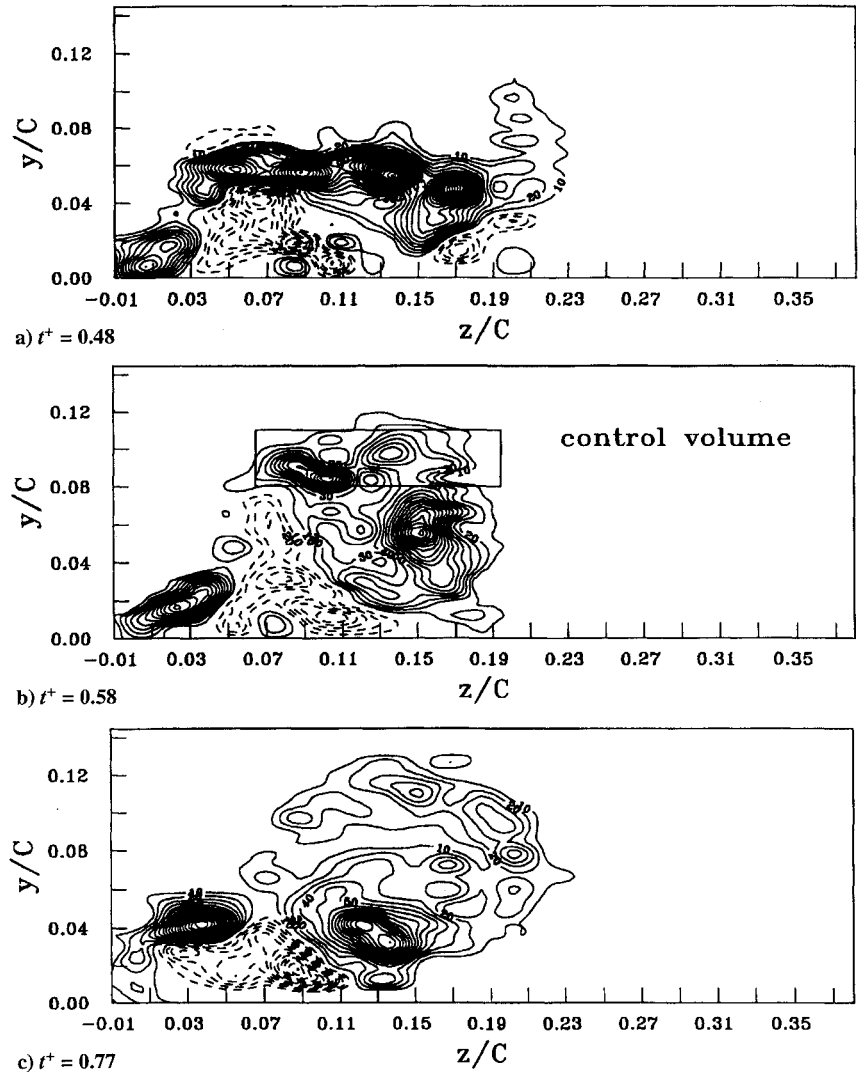

Fig. 14 Variation of the instantaneous vortical structures at 50% chord from the apex, AOA = 12.5 deg.

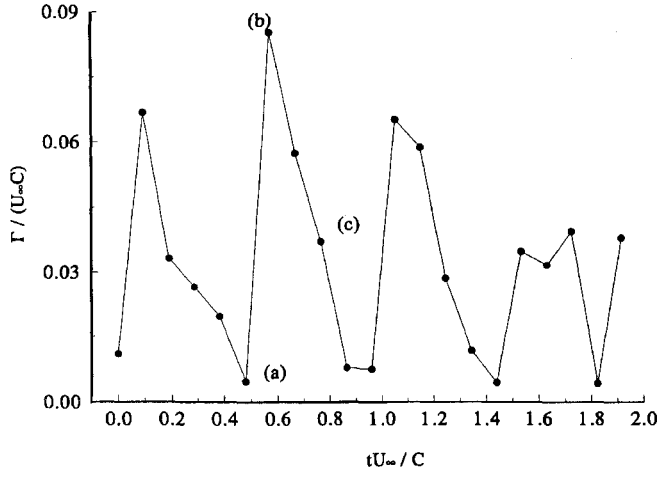

Fig. 15 Variation of the instantaneous circulation measured inside the control volume (Fig. 14b).

inside the vortex breakdown region.[27] A similar variation pattern also observed at the downstream cross section of 58% chord. This suggests that there exists a wavelike disturbance that is propagating along the axial direction before vortex breakdown. As further evidence, the instantaneous velocity and vorticity fields measured along the vortex axis also show a similar wavelike pattern (not shown here). It is speculated that this oscillatory variation is caused by the coherent fluctuations associated with the vortex breakdown further downstream.[27] A more detailed investigation is under way to understand this phenomenon.

Figures 16a and 16b show the averaged vorticity field measured at 92% chord without and with jet control, respectively. Without control, the burst vortex shows little sign of coherence with higher vorticity concentration distributed away from the core region. The peak vorticity level is much lower compared with those measured at the upstream stations with no vortex breakdown (Fig. 16a). This observation is consistent with the flow visualization results that the vortex after breakdown is disorganized and expanded rapidly outward. With control, the leading-edge vortex is not breaking down and its physical appearance is similar to the unburst structure measured at an upstream location without jet control (e.g., compare with Fig. 13b). It is believed that the entrainment effect of the jet relieves the local adverse pressure gradient near the trailing edge that is responsible for the initiation of the vortex breakdown. On the other hand, the accelerated velocity along the core due to the influence of the jet also provides more effective downstream transportation of vorticity, thus stabilizing the leading-edge vortex.

Vortex Core Plane

Figure 17 shows the averaged velocity and associated vorticity fields for flow along vortex core plane without jet control. Before breakdown, the velocity distribution assumes a jet-type profile, with the axial velocity inside the vortex core region overshooting the outer flow by as much as 50%. Further downstream, the axial velocity of the vortex core decelerates drastically, indicated by a flattening of

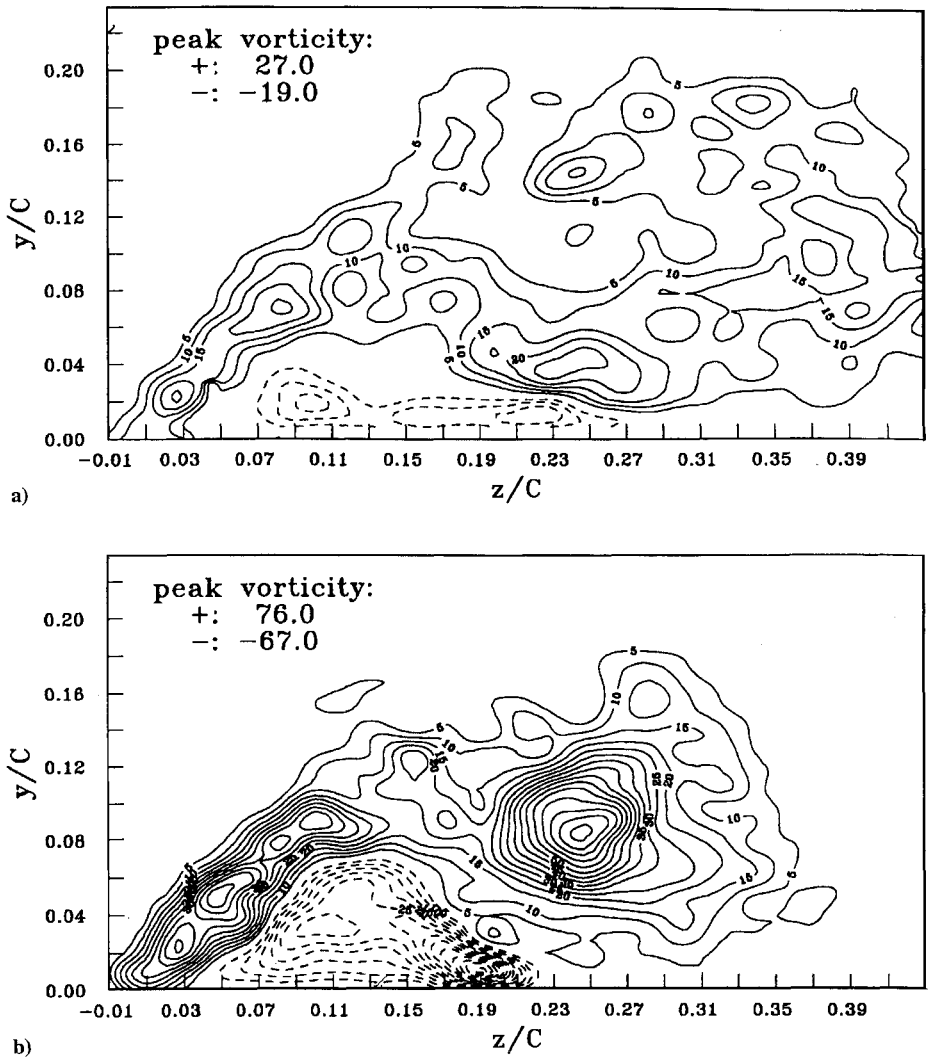

Fig. 16 Averaged vorticity fields at 92% chord from the apex, AOA = 12.5 deg: a) no control and b) with control.

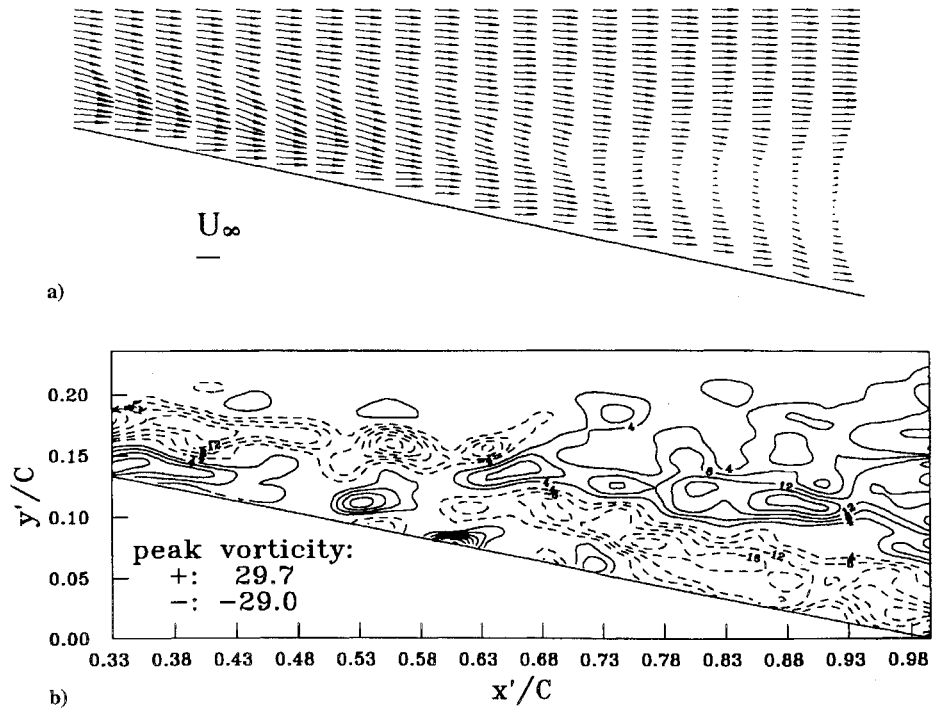

Fig. 17 Averaged a) velocity and b) vorticity fields along the axis of the vortex, AOA = 12.5 deg, no control.

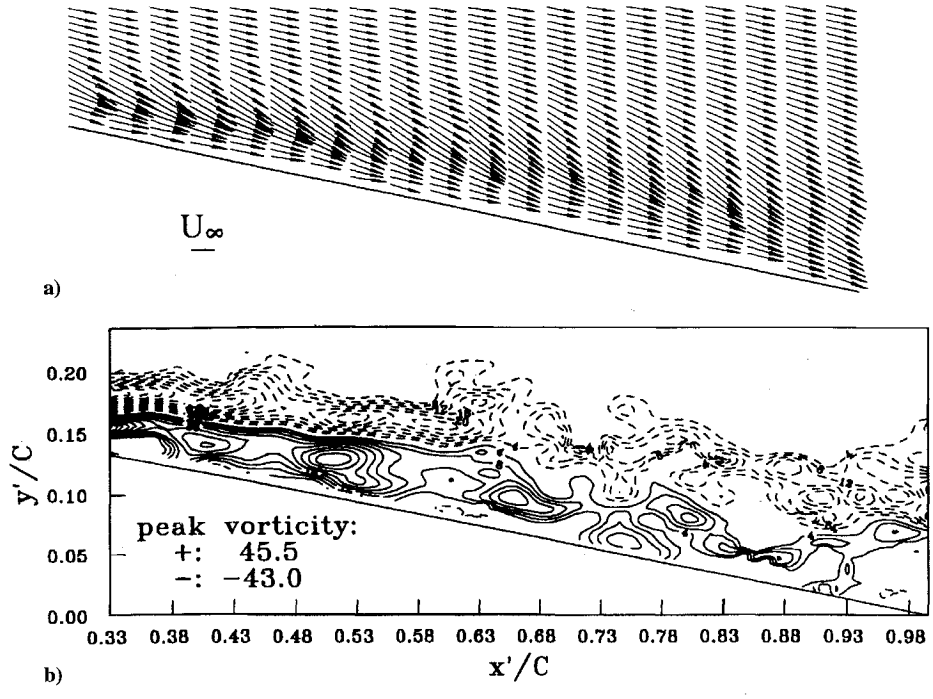

Fig. 18 Averaged a) velocity and b) vorticity fields along the axis of the vortex, AOA = 12.5 deg, with control.

the velocity profile. After breakdown, the wake-type velocity profile shows a large velocity deficit along its center. The most prominent feature of the vorticity plot is the switching of sign of the azimuthal vorticity. That is, in the upstream region, the positive (clockwise, solid contours) vorticity is located near the wall and the negative (counterclockwise, dotted contours) vorticity is on top of the positive vorticity. When the vortex flow undergoes vortex breakdown, the negative vorticity is switched to closer to the wall, whereas the positive vorticity is away from the wall. This phenomenon of vorticity sign change is equivalent to the transition from a jet-type velocity profile to a wake-type velocity profile. It is noted that the location of the switch in sign is consistent with the breakdown location identified by the flow visualization results.

The corresponding case with trailing-edge jet control is shown in Fig. 18. At this condition, no vortex breakdown is observed from flow visualization. Both the velocity and vorticity plot reveal distinct features compared with the corresponding no control case. In the velocity plot, it is seen that the axial velocity in the vortex core region overshoots the outer flow by as much as 100% in specific upstream locations, and the jet-type velocity profile persists all along to the trailing-edge region. The velocity vectors show more tendency to stay attached to the surface as compared with the no control case. In general, the vorticity field shows a more concentrated and a higher vorticity level as compared with the no control case. Downstream of the region where vortex breakdown occurs without control ($X_b/C = 63\%$), there is no switch in sign of vorticity, which is consistent with the observation that no distinguishable vortex breakdown occurs with jet control. However, there is a distinct decrease of the vorticity level through this region and the vortical structure appears to be less organized (Fig. 18b). Furthermore, it is interesting to note that the velocity field also undergoes transition from a jetlike profile with a strong overshoot near the center to a flattened profile at about the same location (Fig. 18a). However, the jetlike profile resumes quickly further downstream. These observations seem to suggest that, although the trailing-edge jet prevents vortex breakdown, the flowfield still experiences an adverse effect that is responsible for the initiation of vortex breakdown in this region without control. However, this adverse effect appears to be confined locally in this region. It is suggested that the favorable effect introduced by the trailing-edge jet entrainment allows the vortex system to overcome the imposed restraint without going through breakdown. As the unburst vortex approaches the trailing edge, the increasing influence of the jet further stabilizes the vortex.

Conclusions

From the dye flow visualization, it has been shown that a vectored, trailing-edge jet has a significant effect in delaying the vortex breakdown on a high AOA delta wing. Within the range tested, the higher the downward vectored angle, the more effective the delay of the vortex breakdown becomes. In some cases, the delay of the vortex breakdown can be as much as 50% chord. The control is most effective when the vortex breakdown occurs near the trailing edge. Strong asymmetric bursting of the leading-edge vortices can be induced by arranging the vectored jet in an asymmetric configuration. The effectiveness of the control jet is also highly dependent on the jet to freestream velocity ratio. Below a certain threshold value, the effect of the control jet is insignificant. Transient pitching motion can also significantly delay the onset of the vortex breakdown. The higher the pitch rate, the higher AOA at which the leading-edge vortices will first experience breakdown on the wing. Transient pitching motion delays the onset of the vortex breakdown and the initial delay is independent of the pitch rates. The use of jet control is found to be effective for the dynamic cases. During the initial pitching-up period, the use of control jets has a dominant influence on the propagation of the vortex breakdown. In general, with jet control, the propagation of the vortex breakdown slows down. From the instantaneous PIV measurements, a quasiperiodic variation of the leading-edge vorticity field is detected even before the vortex breakdown. This variation appears to be related to the strong interaction between the separating shear layer, the primary vortex, and the secondary structure. The secondary vortex appears to play an important role in the development of the leading-edge vortex system. Along the vortex axis, the velocity distribution changes from a jet-type profile to a wake-type profile, signifying the onset of the vortex breakdown. The corresponding azimuthal vorticity field also switches its sign at the vortex breakdown location.

Acknowledgments

This work is supported by the U.S. Air Force Office of Scientific Research under Grant F49620-93-I-0013. We would like to thank A. Krothapalli for his many useful suggestions and discussion concerning this project.

References

[1]Lowson, M. V., Riley, A. J., and Swales, C., "Flow Structure over Delta Wings," AIAA Paper 95-0586, Jan. 1995.

[2]Ng, T. T., Malcolm, G. N., and Lewis, L. C., "Experimental Study of Vortex Flows over Delta Wings in Wing-Rock Motion," *Journal of Aircraft*, Vol. 29, No. 4, 1992, pp. 598–603.

[3]Délery, J. M., "Physics of Vortical Flows,"*Journal of Aircraft*, Vol. 29, No. 5, 1992, pp. 856–876.

[4]Darmofal, D. L., "The Role of Vorticity Dynamics in Vortex Breakdown," AIAA Paper 93-3036, July 1993.

[5]Gursul, I., and Ho, C. M., "Vortex Breakdown over Delta Wings in Unsteady Free Stream," AIAA Paper 93-0555, Jan. 1993.

[6]Kegelman, J. T., and Roos, F. W., "The Flow Field of Bursting Vortices over Moderately Swept Delta wings," AIAA Paper 90-0599, 1990.

[7]Hall, M. G., "Vortex Breakdown," *Annual Review of Fluid Mechanics*, Vol. 4, 1972, pp. 195–218.

[8]Leibovich, S., "Vortex Stability and Breakdown: Survey and Extension," *AIAA Journal*, Vol. 22, No. 9, 1984, pp. 1192–1206.

[9]Lemay, S. P., Batill, S. M., and Nelson, R. C., "Vortex Dynamics on a Pitching Delta Wing," *Journal of Aircraft*, Vol. 27, No. 2, 1990, pp. 131–138.

[10]Rediniotis, O. K., Klute, S. M., Hoang, N. T., and Telionis, D. P., "Dynamic Pitch-Up of a Delta Wing," *AIAA Journal*, Vol. 32, No. 4, 1994, pp. 716–725.

[11]Visbal, M. R., "Structure of Vortex Breakdown on a Pitching Delta Wing," AIAA Paper 93-0434, Jan. 1993.

[12]Visbal, M. R., "Computational Study of Vortex Breakdown on a Pitching Delta Wing," AIAA Paper 93-2974, Jan. 1993.

[13]Hoerner, S. F., and Borst, H. V., "Fluid-Dynamic Lift, Practical Information on Aerodynamic and Hydrodynamic Lift," Hoerner Fluid Dynamics, P.O. Box 342, Brick Town, NJ 08724, 1985, Chap. 5.

[14]Bowers, D. L., "Aerodynamic Effects Induced by a Vectored High Aspect Ratio Nonaxisymmetric Exhaust Nozzle," *Journal of Aircraft*, Vol. 16, No. 8, 1979, pp. 515–520.

[15]Paulson, J. W., "Analysis of Thrust-Induced Effects on the Longitudinal Aerodynamics of STOL Fighter Configurations," *Journal of Aircraft*, Vol. 18, No. 11, 1981, pp. 951–955.

[16]Shih, C., Lourenco, L., Ding, Z., and Krothapalli, A., "Thrust-Induced Effect on a Pitching-Up Delta Wing Flow Field," AIAA Paper 94-1856, 1994.

[17]Helin, H. E., and Watry, C. W., "Effects of Trailing Edge Jet Entrainment on Delta Wing Vortices," *AIAA Journal*, Vol. 32, No. 4, 1994, pp. 802–804.

[18]Nawrocki, D., "Differential and Vectored Trailing Edge Jet Control of Delta Wing Vortices," AIAA Paper 95-0008, Jan. 1995.

[19]Lin, J.-C., and Rockwell, D., "Transient Structure of Vortex Breakdown on a Delta Wing," *AIAA Journal*, Vol. 33, No. 1, 1995, pp. 6–12.

[20]Cipolla, K. M., and Rockwell, D., "Flow Structure on Stalled Delta Wing Subjected to Small Amplitude Pitching Oscillations," *AIAA Journal*, Vol. 33, No. 7, 1995, pp. 1256–1262.

[21]Lourenco, L., Krothipalli, A., and Smith, C., "Particle Image Velocimetry," *Lecture Notes in Engineering 45, Advances in Fluid Mechanics Measurements*, edited by M. Gad-el-Hak, Springer–Verlag, New York, 1989, pp. 127–199.

[22]Shih, C., Lourenco, L., Van Dommelen, L., and Krothapalli, A., "Unsteady Flow Past an Airfoil Pitching at a Constant Rate," *AIAA Journal*, Vol. 30, No. 5, 1992, pp. 1153–1161.

[23]Wentz, W. H., and Kohliman, D. L., "Vortex Breakdown on Slender Sharp-Edges Wings," *Journal of Aircraft*, Vol. 8, No. 3, 1971, pp. 156–161.

[24]Miau, J. J., Chang, R. C., Chou, J. H., and Lin, C. K., "Nonuniform Motion of Leading-Edge Vortex Breakdown on Ramp Pitching Delta Wings," *AIAA Journal*, Vol. 30, No. 7, 1992, pp. 1691–1702.

[25]Ericsson, L. E., and Reding, J. P., "Approximate Nonlinear Slender Wing Aerodynamics," *Journal of Aircraft*, Vol. 14, No. 12, 1977, pp. 1197–1204.

[26]Ericsson, L. E., "Delta Wing Vortex Breakdown Dynamics," AIAA Paper 95-0367, Jan. 1995.

[27]Gursul, I., "Unsteady Flow Phenomena over Delta Wings at High Angle of Attack," *AIAA Journal*, Vol. 32, No. 2, 1994, pp. 225–231.